Chain Packing in the Inverted Hexagonal Phase of Phospholipids: A Study by X-ray Anomalous Diffraction on Bromine-labeled Chains

Deng Pan,[†] Wangchen Wang,[†] Wenhan Liu,[§,†] Lin Yang,[‡] and Huey W. Huang*,[†]

Contribution from the Department of Physics & Astronomy, Rice University, Houston, Texas 77251, and National Synchrotron Light Source, Brookhaven National Laboratory, Upton, New York 11973.

Received November 26, 2005; E-mail: hwhuang@rice.edu

Abstract: Although lipid phases are routinely studied by X-ray diffraction, construction of their unit cell structures from the diffraction data is difficult except for the lamellar phases. This is due to the well-known phase problem of X-ray diffraction. Here we successfully applied the multiwavelength anomalous dispersion (MAD) method to solve the phase problem for an inverted hexagonal phase of a phospholipid with brominated chains. Although the principle of the MAD method for all systems is the same, we found that for lipid structures it is necessary to use a procedure of analysis significantly different from that used for protein crystals. The inverted hexagonal phase has been used to study the chain packing in a hydrophobic interstice where three monolayers meet. Hydrophobic interstices are of great interest, because they occur in the intermediate states of membrane fusion. It is generally believed that chain packing in such a region is energy costly. Consequently, it has been speculated that the inverted lipid tube is likely to deviate from a circular shape, and the chain density distribution might be nonuniform. The bromine distribution obtained from the MAD analysis provides the information for the chain packing in the hexagonal unit cell. The intensity of the bromine distribution is undulated around the unit cell. The analysis shows that the lipid chains pack the hexagonal unit cell at constant volume per chain, with no detectable effect from a high-energy interstitial region.

I. Introduction

Lipid molecules form a great variety of soft crystalline structures. This was known since the 1960s through the X-ray diffraction studies of lipid-water systems pioneered by Luzzati and co-workers.[1] However, with the exception of lamellar phases in which lipid molecules form a bilayer in unit cell, phase determinations for diffraction from the soft crystalline structures are tedious and somewhat uncertain.[2] In this paper, we will use X-ray anomalous diffraction to study the inverted hexagonal phase of a bromine-labeled phospholipid so as to determine the phases of the diffraction amplitudes. The success of this application opens the possibility of solving the phase problem for other more complicated structures. The electron density distribution of the bromine labels shows how the lipid chains are packed in a hexagonal unit cell, and thus reveals a principle of chain packing in a nonlamellar structure. This problem was first investigated by Turner and Gruner[3] with normal X-ray

diffraction, but their results were somewhat tentative for two reasons. One was that the phase determination by model fitting and other methods was not unambiguous. Another was that lipid chains without labels are of low electron density; therefore their distribution could not be seen clearly. A more recent attempt by neutron diffraction[4] solved the phase problem successfully. However neutron diffraction has a lower resolution than X-ray, and again the scattering length density of the chains was low.

The knowledge of how lipid chains pack in small-size nonlamellar lipid structures, where the radius of curvature is of the same order of magnitude as the membrane thickness, is of considerable importance in biology. While large-scale shape transitions of lipid bilayers (where the radius of curvature ≫ membrane thickness) have been extensively studied and their principles well established,[5,6] the energetics of small-scale shape changes are not as well understood. The reason is that large-scale shape changes are entirely determined by the geometry (and topology) of the interface that is governed by the Helfrich free energy.[5,6] But on small scales the energetics also depends on how the chains pack into a particular structure. Perhaps the most important example is the structural changes of lipid bilayers during membrane fusion. Recent studies[7] have shown that varieties of protein-mediated fusions all involve a series of

[†] Rice University.

[‡] Brookhaven National Laboratory.

[§] On leave from Department of Physics, University of Sciences and Technology of China, Hefei, China.

(1) (a) Luzzati, *V. Biological Membranes*; Chapman, D., Ed.; Academic Press: New York, 1968; pp 71−123. (b) Tardieu, J.; Luzzati, V.; Reman, F. C. K. *Mol. Biol.* **1973**, *75*, 711−733.

(2) (a) Luzzati, V.; Tardieu, A.; Taupin, D. *J. Mol. Biol.* **1972**, *64*, 269−286. (b) Mariani, P.; Luzzati, V.; Delacroix, H. *J. Mol. Biol.* **1988**, *204*, 165−189.

(3) Turner, D. C.; Gruner, S. M. *Biochemistry* **1992**, *31*, 1340−1355.

(4) Ding, L.; Liu, W. H.; Wang, W. C.; Glinka, C. J.; Worcester, D. L.; Yang, L.; Huang, H. W. *Langmuir* **2004**, *20*, 9262−9269.

(5) Helfrich, W. Z. *Naturforsch.* **1973**, *28c*, 693−703.

(6) Lipowsky, R. *Curr. Opin. Struct. Biol.* **1995**, *5*, 531−540.

structural changes of lipid bilayers similar to what takes place during the fusion between two lipid vesicles. The lipid structure of a fusion intermediate state has also been identified.[8] Thus, it is generally believed that the energetic pathway of the lipid transformation will serve as a guide to understand the actions of membrane fusion proteins.[9] However, not knowing the chain configurations in the intermediate structure has led to uncertainties of its energetics.[10]

The inverted hexagonal (H_{II}) phase is perhaps the simplest nonlamellar structure. Within the Wigner−Seitz cell, it is assumed that a water core along the hexagonal axis is surrounded by the lipid headgroups with their chains distributed radially toward the boundary of the cell.[1] Although the unit cells of the H_{II} phase are often depicted as circular lipid tubes, it has been speculated that the interface is likely to deviate from a circular shape,[11,12] and also that the chain density distribution might be nonuniform near the boundary.[3,11,13] This speculation is based on the fact that the distance from a circular interface to the unit cell boundary is not constant. The lipid chains have to stretch farthest near the interstitial corner. It has been argued that the energy cost of chain stretching is high, therefore the circular symmetry could be broken.[3,13] Our result will indeed show a noncircular distribution of bromine atoms, but we will also find that lipid chains pack the hexagonal space at constant chain density with no detectable effect of stretching stress.

The method of multiwavelength anomalous dispersion (MAD)[14] is a powerful tool for separating the diffraction by the label (heavy) atoms from that of the host molecules, and subsequently solving the phase problem of diffraction. However, this commonly used method in protein crystallography[15] does not apply to lipid systems in a straightforward manner. In the standard method,[14] one separates the label amplitudes from the host amplitudes by solving a set of equations using the intensities measured at energies below and above the absorption edge of the label atom. This requires a precise correction for X-ray absorption by the sample, which is difficult to do for the lipid systems. Therefore, we measured the diffraction only at energies below the absorption edge, where the X-ray absorption is relatively energy-independent. We then used a method similar to the D_2O/H_2O exchange in neutron diffraction,[4,16] that allowed

us to determine the magnitudes of the label and host amplitudes, as well as the phase relation between them. Thus, we reduced the phase problem of the lipid diffraction to that of the label-atoms alone. Essentially, the problem was solved by building a model of label distribution to fit the Patterson map derived from the data.

As far as we know, this is the first attempt to solve the phase problem for a nonlamellar lipid structure by the MAD method. (The MAD method was used for a problem in the lamellar phase.)[17] We will first describe the experimental method and in the second part analyze the chain packing in the inverted hexagonal phase.

II. Experimental Methods

IIA. Materials. 1,2-Distearoyl(dibromo)-sn-Glycero-3-Phosphocholine (abbreviated as di18:0(9−10dibromo)PC) and cholesterol were purchased from Avanti Polar Lipids Inc. (Alabaster, AL). Silicon wafers (⟨100⟩ surface, P-doped), 300 μm thick, were purchased from Virginia Semiconductor (Fredericksburg, VA). All materials were used as delivered.

IIB. Sample Preparation. The diffraction sample, i.e., the inverted hexagonal phase of the mixture of di18:0(9−10dibromo)PC and cholesterol in the molar ratio of 2:1 was prepared as follows. The lipid sample was first prepared in the form of parallel hydrated lipid bilayers on a solid substrate. At 25 °C and in full hydration, the lipid mixture is in the L_α phase. The sample was then phase transitioned to the inverted hexagonal phase by lowering the level of hydration in a humidity chamber.[18]

The preparation for oriented samples followed the method described in Ludtke et al.[19] Essentially, the lipid mixture was first dissolved in a 1:1 trifluoroethanol (TFE)-chloroform solvent and then uniformly deposited onto a clean, flat silicon substrate. The organic solvent was evaporated in a vacuum or open air. A total of 300 μg of di18:0(9−10dibromo)PC and 52.5μg of cholesterol were spread over a 10 × 20 mm^2 silicon wafer. The deposit was then hydrated with saturated water vapor and incubated in an oven at 35 °C overnight.

IIC. Experimental Setup. X-ray experiment was performed at the beamline X21 of the National Synchrotron Light Source, Brookhaven National Laboratory (Upton, NY). The setup was similar to the one described in Yang and Huang.[18] The X-ray beam was collimated by two sets of slits before the sample chamber, resulting in a beam size of ∼0.5 mm × ∼0.5 mm at the sample.

IID. Anomalous Scattering Factor of Bromine. It is well-known that the absorption edge and the scattering factor near the edge are influenced by the chemical environment of the atom. Therefore, one measures the anomalous scattering factor of the label atom in the actual sample. The absorption spectrum was measured in the fluorescence mode. The incident beam intensity was monitored by an ion chamber. The fluorescence was measured at 90° using a PIPS detector. Prior to the measurement, the energy dependence of the PIPS detector was calibrated by an ion chamber.

After the Br K-edge was identified at 13.474 keV, the experimental absorption curve was measured over both sides of the edge. The absorption curve was then converted to the imaginary scattering factor f by using the theoretical values calculated by Cromer.[20] The real part f' was calculated by the dispersion relation (Figure 1). The calculations of f' and f'' were carried out using the CHOOCH program by Evans.[21] Eight energies were chosen with a differential $\Delta f' = 0.5$ (in the unit of electron) for each successive energy as shown in Figure 1.

(7) (a) Reese, C.; Heise, F.; Mayer, A. *Nature* **2005**, *436*, 410−414. (b) Giraudo, C. G.; Hu, C.; You, D.; Slovic, A. M.; Mosharov, E. V.; Sulzer, D.; Melia, T. J.; Rothman, J. E. *J. C. Biol.* **2005**, *170*, 249−260. (c) Zaitseva, E.; Mittal, A.; Griffin, D. E.; Chernomordik, L. V. *J. Cell Biol.* **2005**, *169*, 167−177. (d) Xu, Y.; Zhang, F.; Su, J.; McNew, J. A.; Shin, Y.-K. *Nature Struct. Mol. Biol.* **2005**, *12*, 417−422.
(8) Yang, L. and Huang, H. W. *Science* **2002**, *297*, 1877−1879.
(9) (a) Lentz, B. R.; Lee, *J. Mol. Membrane Biol.* **1999**, *16*, 279−296. (b) Chernomordik, L. V.; Kozlov, M. M. *Annu. Rev. Biochem.* **2003**, *72*, 175−207.
(10) (a) Markin, V. S.; Albanes, J. P. *Biophys. J.* **2002**, *82*, 693−712. (b) Kozlovsky, Y.; Koxlov, M. *Biophys. J.* **2002**, *82*, 882−895. (c) May, S. *Biophys. J.* **2002**, *83*, 2969−2980.
(11) Kirk, G. L.; Gruner, S. M. *J. Phys (Paris)* **1985**, *46*, 761−769.
(12) Seddon, J. M. *Biochim. Biophys. Acta* **1990**, *1031*, 1−69.
(13) Kirk, G. L.; Gruner, S. M.; Stein, D. E. *Biochemistry* **1984**, *23*, 1093−1102.
(14) Karle, J. *Phys. Today* **1989**, *42*, 22−29.
(15) (a) Kahn, R.; Fourme, R.; Bosshard, R.; Chiadmi, M.; Risler, J. L.; Dideberg, O.; Wery, J. P. *FEBS Lett.* **1985**, *179*, 133−137. (b) Hendrickson, W. A.; Smith, J. L.; Phizackerley, R. P.; Merritt, E. A. *Proteins: Struct. Funct. Genet.* **1988**, *4*, 77−88. (c) Guss, J. M.; Merritt, E. A.; Phizackerley, R. P.; Hedman, B.; Murata, M.; Hodgson, K. O.; Freeman, H. C. *Science* **1988**, *241*, 806−811. (d) Murthy, H. M. K.; Hendrickson, W. A.; Orme-Johnson, W. H.; Merritt, E. A.; Phizackerley, R. P. *J. Biol. Chem.* **1988**, *263*, 18430-18436. (e) Hendrickson, W. A.; Pahler, A.; Smith, J. L.; Satow, Y.; Merritt, E. A.; Phizackerley, R. P. *Proc. Natl Acad. Sci. USA,* **1989**, *86*, 2190−2194.
(16) Ding, L.; Weiss, T. M.; Fragneto, G.; Liu, W.; Yang, L.; Huang, H. W. *Langmuir* **2005**, *21*, 203-210.
(17) Liu, W.; Teng, T. Y.; Wu, Y.; Huang, H. W. *Acta Crystallogr.* **1991**, *A47*, 553−559.
(18) Yang, L.; Huang, H. W. *Biophys. J.* **2003**, *84*, 1808−1817.
(19) Ludtke, S.; He, K.; Huang, H. W. *Biochemistry* **1995**, *34*, 16764−16769.
(20) Cromer, D. T.; Libermann, D. *J. Chem. Phys.* **1970**, *53*, 1891−1898.
(21) (a) Evans, G.; Pettifer, R. F. *Rev. Sci. Instr.* **1996**, *67*, 3428−3433. (b) Evans, G.; Pettifer, R. F. *J. Appl. Crystallogr.* **2001**, *34*, 82−86.
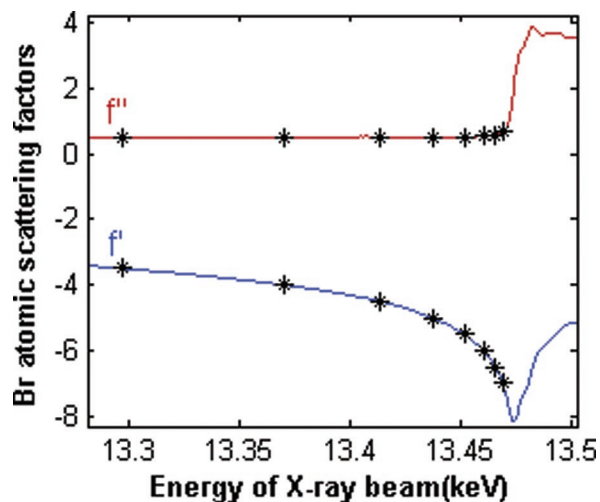
Figure 1. Anomalous scattering factor of bromine atom. The K-edge is at 13.474 keV. Asterisks mark the selected energies for MAD measurements.
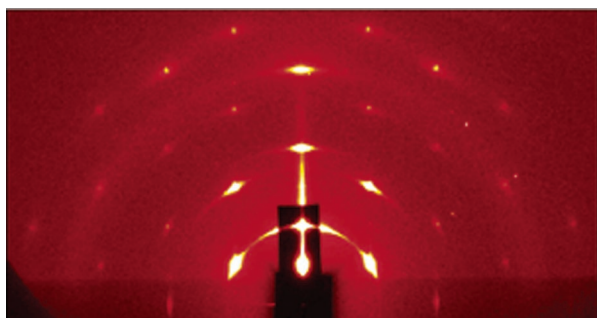

Figure 2. Diffraction pattern of the inverted hexagonal phase measured by reflection.

IIE. Diffraction Patterns and Data Reduction. A MarCCD detector (MAR, Evanston, IL) was used to capture the diffraction pattern. Its energy dependence was also calibrated with an ion chamber detector. A helium beam path between the sample chamber and the detector was used to reduce the scattering by air. Since the lipid started as a stack of bilayers, the hexagonal phase was composed of lipid tubes parallel to the substrate. The tubes were organized in a two-dimensional hexagonal lattice with the lattice plane oriented vertical to the substrate. The horizontal orientation of lattice domains is however random (the sample was a two-dimensional powder). Therefore, each Bragg peak of the hexagonal lattice forms a Bragg ring parallel to the substrate, except for the meridional peaks. In general, as described in Yang and Huang,[18] a complete diffraction pattern requires three diffraction geometries: A small angle reflection will intercept all the Bragg rings except the ones with $q_z = 0$. The Bragg rings at $q_z = 0$ need to be measured at a transmission geometry. And finally, the meridional peaks need to be measured by a $\theta - 2\theta$ scan.

However in our case, due to the hexagonal symmetry of the unit cell, a reflection measurement at a small incident angle ($\sim0.5°$ relative to the substrate) was sufficient (Figure 2). The Bragg rings captured by the reflection are shown as solid circles in Figure 3. The reciprocal lattice points shown as open circles in Figure 3 are each related to a solid-circle lattice point by symmetry. (The meridional peaks in Figure 2 were due to the mosaic nature of the sample and the fact that their Bragg conditions were nearly satisfied. If we were to use the meridional peaks in analysis, their integrated intensities would need to be measured by a $\theta - 2\theta$ scan.[18] In contrast, the integrated intensities of the off-meridional peaks, that form the Bragg rings, are correctly measured by the powder reflection.) The same reflection (Figure 2) was measured at the eight chosen energies (Figure 1) below the Br K-edge.

Extracting integrated peak intensities from the raw data followed the method described in Yang and Huang[18] and Ding et al.[16] The steps
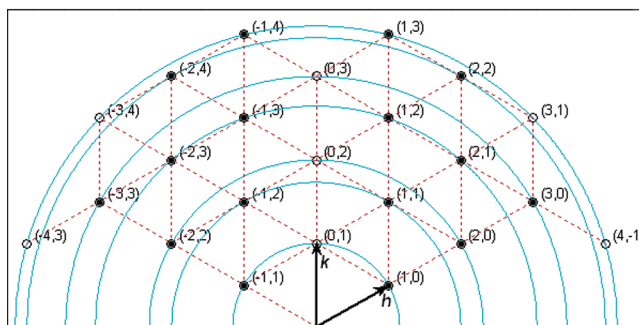
Figure 3. Detected Bragg peaks on the hexagonal reciprocal lattice. The peaks shown as solid circles were measured and analyzed. (3,1), (−3,4), (4,−1), and (−4,3) were detected but too weak to be measured accurately. The lattice points at open circles are related to solid circles by symmetry.

include background removal and corrections for polarization, the Lorentz factor, diffraction volume, and absorption. In addition, for multiwavelength measurements, one needs to correct the intensities for the wavelength dependence: the measured intensity is proportional to λ^3.[22] The technical details of the MAD measurement and analysis will be published elsewhere.

IIF. MAD Analysis. The diffraction amplitude of a system containing atoms of an element with anomalous scattering factor $f = f^n + f_\lambda' + if_\lambda''$ is written as

$$F_\lambda = \sum_j f_j^n \exp(iq \cdot r_j) + \sum_k (f_k^n + f_\lambda' + if_\lambda'') \exp(iq \cdot r_k) =$$

$$F_0 + \frac{f_\lambda' + if_\lambda''}{f^n} F_2 \quad (1)$$

where q is the scattering vector. f_j^n is the normal scattering factor of atom j at position r_j. The index j includes all atoms except for the labels. The index k includes all the label (anomalous) atoms. $F_0 = \sum_j f_j^n \exp(iq \cdot r_j) + \sum_k f_k^n \exp(iq \cdot r_k)$ is the normal diffraction amplitude of the whole system. $F_2 = \sum_k f_k^n \exp(iq \cdot r_k)$ is the normal diffraction amplitude of the label atoms alone. We will assume that the unit cell of the inverted hexagonal phase is centrosymmetric, so that both F_0 and F_2 are real quantities. The following analysis will test whether this assumption is valid. From eq 1, we have $|F_\lambda|^2 = [F_0 + (f_\lambda'/f^n) F_2]^2 + (f_\lambda''/f^n)^2 F_2^2$. The second term is about 1% of the first term, because for energies below the absorption edge f_λ'' (~0.5) is about 1/10 of $|f'|$ (Figure 1). Therefore we have the approximate relation

$$|F_\lambda| \approx \pm \left(F_0 + \frac{f_\lambda'}{f^n} F_2 \right) \quad (2)$$

We now plot $|F_\lambda|$ against $-f_\lambda'/f^n$ (or $|f_\lambda'|/f^n$) for each peak (Figure 4). The data for every peak appear to satisfy a linear relation (i.e., a straight line). Therefore, we conclude that both the assumption of centrosymmetry and the linear approximation eq 2 are valid. In each plot, we fitted the average data with a straight line. The standard deviation ϵ of the slope in the fit will be used in the following analysis. From eq 2, we see that the intercept of the fitted line gives $|F_0|$; the magnitude of the slope gives $|F_2|$; and the sign of the slope is the sign of $-F_0/F_2$ (Table 1). The individual signs of F_0 and of F_2 remain undetermined.

Results and Discussion

At 25 °C and in full hydration, the phospholipid di18:0-(9−10dibromo)PC is in the fluid lamellar (L_α) phase. We induced phase transitions by lowering the relative humidity of the air in equilibrium with the sample at constant temperature

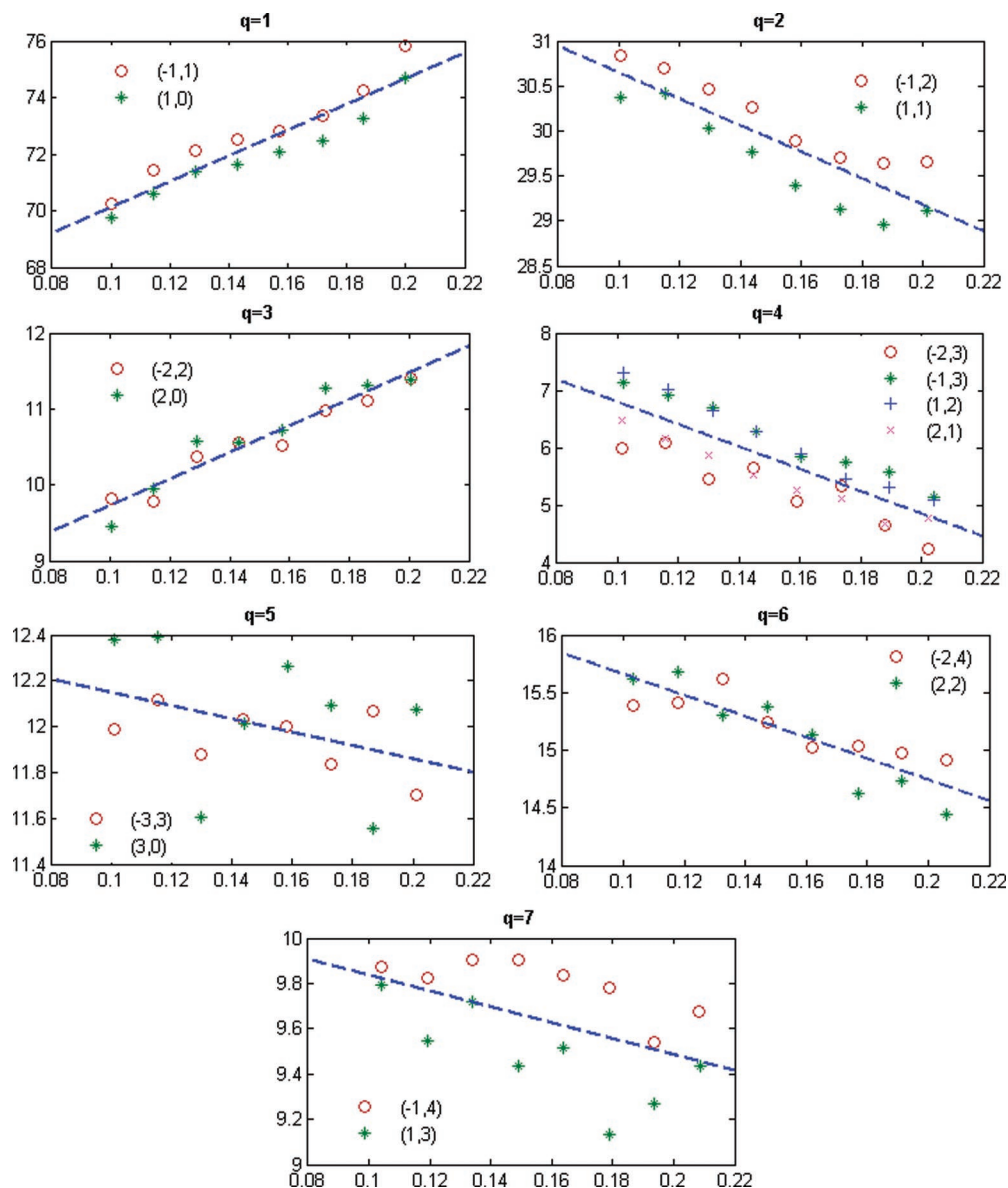(22) Warren, B. E. *X-ray Diffraction*; Dover: New York 1969; p. 44.

Figure 4. Plotting eq 2 for seven independent peak intensities listed in Table 1. For each panel, the ordinate is $|F_\lambda|$ and the abscissa is $|f_\lambda'|/f^n$. From the slope and intercept of the linear fit, we obtain $|F_0|$ and $|F_2|$ and the ratio F_0 / F_2. The results are listed in Table 1.

(25 °C). Pure 18:0(9−10dibromo)PC exhibits a phase transition to the rhombohedral phase[8,18] below ∼60%RH. No other phases were observed between 40% and 100%RH. However, if cholesterol is added to di18:0(9−10dibromo)PC (in this experiment at the 2:1 PC:cholesterol molar ratio) two more phases appear in low hydrations. From high RH to low RH, the mixture changed from the L_α phase first to the rhombohedral phase at 70% RH and then to a distorted hexagonal phase[23] at 60%RH and finally to an inverted hexagonal (H_{II}) phase below 44%RH. It is well-known that addition of cholesterol promotes the H_{II} phase or enhances the negative curvature of the lipid mixture.[24] The system described below is the homogeneous mixture of 18:0(9−10dibromo)PC and cholesterol at 2:1 molar ratio at 25 °C and 40%RH. The diffraction from this system showed a 2D hexagonal lattice with the lattice constant $D = 44.933$Å. We will now reconstruct the electron distributions within a Wigner-Seitz cell.

7 independent Bragg peaks were detected from the H_{II} phase by X-ray (Figure 3), denoted by hexagonal indices (*h, k*) in Table 1. All the indices related by the hexagonal symmetry and by the mirror symmetry with respect to the axis (*1,0*) and axis (*1,1*) are grouped under each of the seven peaks (Table 1). The diffraction patterns were measured at 8 different energies slightly below the K-edge of Br atom at 13.474 keV. Each diffraction amplitude is a linear combination of the normal (nonanomalous) diffraction amplitude of the whole lipid F_0 and the normal diffraction amplitudes of Br atoms alone F_2. The anomalous analysis assumes that the unit cell is centrosymmetric, so that the phase angles of all normal amplitudes are either zero or π; that means each normal amplitude is either positive or negative. The coefficient multiplying to F_2 depends on the real part of the scattering factor of Br, which we have experimentally measured. Thus, we were able to use the changes of the diffraction intensity with energy to separate $|F_2|$ and $|F_0|$ (Figure

(23) Yang, L.; Ding, L.; Huang, H. W. *Biochemistry* **2003**, *42*, 6631−6635.

(24) Chen, Z.; Rand, R. P. *Biophys. J.* **1997**, *73*, 267−276.

Table 1. Detected Bragg Peaks and Results of MAD Analysis

i	1	2	3	4	5	6	7
(h,k)'s included in the calculation	(−1,1)[a] (1,0)[a] (0,1) (1,−1) (0,−1) (1,0)	(−1,2)[a] (1,1)[a] (2,−1) (1,−2) (−1,−1) (−2,1)	(−2,2)[a] (2,0)[a] (0,2) (2,−2) (0,−2) (−2,0)	(−2,3)[a] (−1,3)[a] (1,2)[a] (2,1)[a] (3,−1) (3,−2) (2,−3) (1,−3) (−1,−2) (−2,−1) (−3,1) (−3,2)	(3,0)[a] (−3,3)[a] (0,3) (0,−3) (−3,0) (3,−3)	(−2,4)[a] (2,2)[a] (4,−2) (2,−4) (−2,2) (−4,2)	(−1,4)[a] (1,3)[a] (3,1) (4,−1) (4,−3) (3,−4) (1,−4) (−1,−3) (−3,−1) (−4,1) (−4,3) (−3,4)
$q = \sqrt{h^2 + k^2 + hk}$	1	$\sqrt{3}$	2	$\sqrt{7}$	3	$2\sqrt{3}$	$\sqrt{13}$
$|F_2|^2$	2070	215	305	379	8.36	83.5	12.3
F_0/F_2	1.44	−2.19	0.457	−0.449	−4.30	−1.81	−2.90
ϵ_i: standard deviation of $|F_2|$	4.17	1.53	1.58	0.686	1.74	0.978	0.953

[a] The peaks at (h,k)[a] were measured and analyzed. All (h,k)'s in each column have the same amplitude by symmetry.
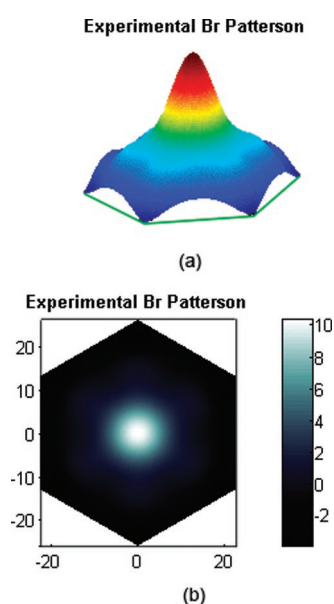

Figure 5. Patterson function for the bromine distribution. (a) 3-D view. (b) 2-D top view. The horizontal x, y coordinates are in the unit of Å. The vertical scale for the value of the Patterson function is arbitrary.

4). In addition, the sign of the amplitude ratio F_0/F_2 was also determined from the analysis, so that knowing the phases of F_2 will determine the phases of F_0. The difficult problem of determining the phases for the whole lipid is now reduced to the simpler problem of determining the phases for the Br distribution alone. Table 1 shows the results of the MAD analysis that extracted $|F_2|$ and F_0/F_2 from the diffraction data.

Patterson Map for Bromine Distribution. We use the amplitudes $|F_2|$ to build the Patterson function of the Br distribution

$$P(r,\theta) = \sum_{(h,k)} |F_2(h,k)|^2 \cos\left\{\frac{2\pi}{D}r\left[\left(\frac{\sin\theta}{\sqrt{3}} + \cos\theta\right)h + \left(\frac{2}{\sqrt{3}}\sin\theta\right)k\right]\right\} \quad (3)$$

and display it in Figure 5. The fact that the Patterson function

contains only one single peak implies that the Br distribution is localized at one radius and the width of the peak indicates the width of the Br distribution around that radius. Therefore, we build our initial model as a circular ring of Br distribution around the center of the unit cell. In a reference unit cell, we define

$$G[x_c,y_c] = \exp\left[\frac{-(\sqrt{(r\cos\theta - x_c)^2 + (r\sin\theta - y_c)^2} - r_o)^2}{2\sigma^2}\right] \quad (4)$$

where (r, θ) are the polar coordinates with the origin at the center of the reference unit center. $[x_c,y_c]$, referred to the same origin, are the coordinates of the center of a unit cell, which is either the reference unit cell or one of its adjacent unit cells. Within each unit cell, Br atoms are radially Gaussian-distributed, peaked at the radius r_o with a width σ. Equation 4 describes the Br distribution in an isolated unit cell. To obtain the Br distribution in a lattice, we need to include the density contribution of the six adjacent unit cells. Thus the electron density measured by X-ray diffraction in the [0,0] unit cell is calculated from

$$\rho_{mod}^{Br}(r,\theta) = G[0,0] + G[D,0] + G\left[\frac{D}{2}, \frac{\sqrt{3}D}{2}\right] +$$
$$G\left[-\frac{D}{2}, \frac{\sqrt{3}D}{2}\right] + G[-D,0] + G\left[-\frac{D}{2}, -\frac{\sqrt{3}D}{2}\right] +$$
$$G\left[\frac{D}{2}, -\frac{\sqrt{3}D}{2}\right] \quad (5)$$

The model amplitudes are calculated by

$$F_{mod}^{Br}(h,k) =$$
$$\iint_{r,\theta} \rho_{mod}^{Br} P(r,\theta) \cdot \cos\left\{\frac{2\pi}{D}r\left[\left(\frac{\sin\theta}{\sqrt{3}} + \cos\theta\right)h + \left(\frac{2}{\sqrt{3}}\sin\theta\right)k\right]\right\} \cdot r dr d\theta \quad (6)$$

where the integration is over one unit cell. We adjusted the model parameters r_o and σ until we obtained the best fit between
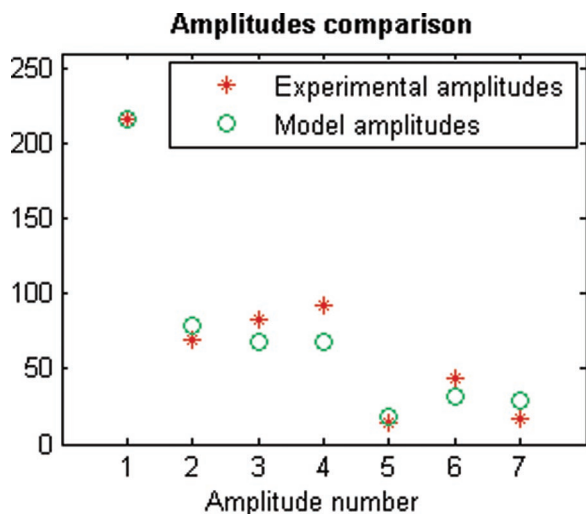
Figure 6. Comparison of the magnitude of amplitude between the initial model and experiment. The amplitude nos. 1 to 7 are given in Table 1. The magnitudes are normalized to each other for amplitude no. 1.

the model amplitudes $|F^{Br}_{mod}(h,k)|$ and the seven experimental amplitudes $|F_2(h,k)|$ listed in Table 1 (see Figure 6).

Reconstruction of Bromine Electron Density in a Unit Cell. We now apply the phases determined from the initial model, eq 6, to the experimental amplitude F_2 to reconstruct the Br electron density distribution in the unit cell.

$$\rho^{Br}_{exp}(r,\theta) = \sum_{(h,k)} F_2(h,k) \cdot \cos\left\{\frac{2\pi}{D} r\left[\left(\frac{\sin\theta}{\sqrt{3}} + \cos\theta\right)h + \left(\frac{2}{\sqrt{3}}\sin\theta\right)k\right]\right\} \quad (7)$$

where the sum is over all indices (h, k) included in the second row of Table 1 for the seven independent amplitudes. The result is plotted in Figure 7.

Comparing Figure 7 (the experimental Br distribution determined by the model phases) with the initial model (as described by eq 6), we note that: (a) the Gaussian width is not symmetric with respect to $r < r_o$ and $r > r_o$; (b) the height of the distribution is undulated as a function of the azimuthal angle θ. We would like to test if these are the true features of the Br distribution. We would believe that they are the true features, if the agreement between the model and experiment can be improved by applying the features to the model.

First we define a function that measures the agreement between the model and the experiment.[25]

$$T = \frac{\left[\sum_i \frac{1}{\epsilon_i^2}\left|F^{exp}_i\right| \cdot \left|F^{mod}_i\right|\right]^2}{\sum_i \frac{1}{\epsilon_i^2}(F^{exp}_i)^2 \cdot \sum_i \frac{1}{\epsilon_i^2}(F^{mod}_i)^2} \quad (8)$$

where F^{exp}_i and F^{mod}_i are the experimental and model amplitudes, respectively. ϵ_i is the standard deviation for extracting

(25) (a) Saldin, D. K.; Harder, R.; Vogler, H.; Moritz, W.; Robinson, I. K. *Comput. Phys. Comm.* **2001,** *137,* 12−24. (b) Pannu, N. S.; Read, R. J. *Acta Crystallogr.* **1996,** A52, 659−668.
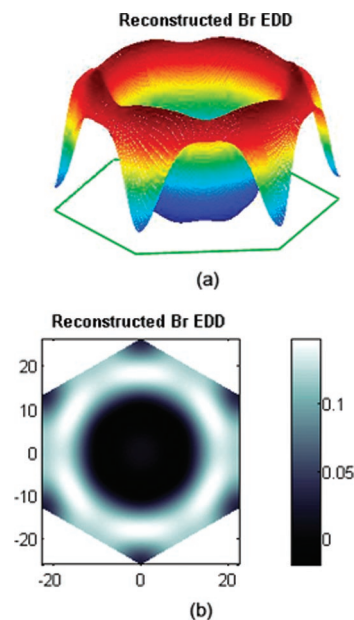

Figure 7. Electron density distribution (EDD) of bromine atoms reconstructed using the phases determined from the model. (a) 3-D view. (b) 2-D top view. The horizontal x, y coordinates are in the unit of Å. The vertical scale for the electron density is e/Å³.
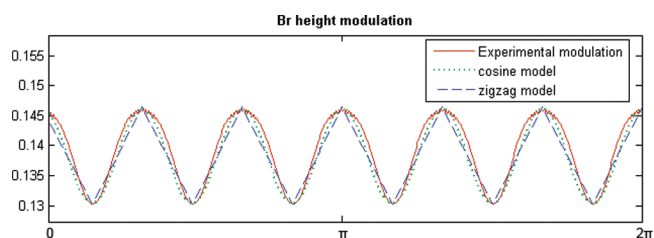

Figure 8. Height undulation of the bromine distribution measured at the peak radius $r = 18.0$ Å in Figure 7. The abscissa is the azimuthal angle θ. The unit of the ordinate is e/Å³.

Table 2. Model Refinements

d	σ_i	σ_o	h	$A(\theta)$	T	remarks
18.0	3.5		1		0.96622	initial model
18.0	3.3	3.4	0.90	linear	0.97175	zigzag model
18.0	3.3	3.4	0.90	cosine	0.97180	cosine model
18.0	3.35	3.44	0.89	cosine	0.97229	the best fit model

F^{exp}_i from the raw data (see IIF MAD analysis). The value of T is ≤ 1, with 1 being the perfect agreement between model and experiment. The initial model gives a $T = 0.96622$.

We modified our model to the following

$$G[x_c, y_c] = A(\theta) \exp\left[\frac{-\left(\sqrt{(r\cos\theta - x_c)^2 + (r\sin\theta - y_c)^2} - r_o\right)^2}{2\sigma^2}\right] \quad (9)$$

where $\sigma = \sigma_-$ or σ_+ for $\sqrt{(r\cos\theta - x_c)^2 + (r\sin\theta - y_c)^2} - r_o < 0$ or > 0, respectively. The factor $A(\theta)$ is to modulate the height. The solid line in Figure 8 shows the height modulation of the Br distribution shown in Figure 7. We shall approximate this height modulation by two models shown in the same graph: a zigzag model and a cosine model. In Table 2, the results of the refinements show a progressive improvement from the initial model to the zigzag model and to the cosine model as the T
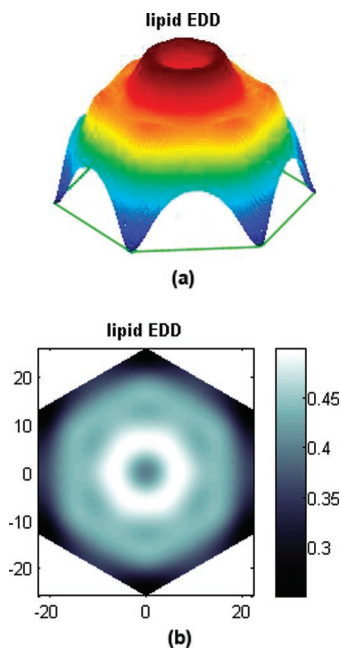
Figure 9. Electron density distribution of the 2:1 mixture of di18:0-(9−10dibromo)PC and cholesterol in a unit cell of the inverted hexagonal phase. (a) 3-D view. (b) 2-D top view. The horizontal x, y coordinates are in the unit of Å. The vertical scale for the electron density is e/Å³.

Figure 10. (a) The green line shows the unit cell of the inverted hexagonal phase (the *x*, *y* coordinates in Å). The red line gives the equivalent radius $R^*(\theta)$ constructed such that the area in red is proportional to the number of lipid chains distributed between θ and $\theta + d\theta$. The closeness of the green and red lines is an indication that the lipid chains pack the hexagonal unit cell at constant volume per chain. (b) The average lipid is composed of 1/3 cholesterol and 2/3 di18:0(9−10dibromo)PC. (The image of the molecular model for di18:0(9−10dibromo)PC was taken from http://www.avantilipids.com/. The blue atoms are bromines.) There are 12.6 average molecules in a unit cell cylinder of 8.6Å in height. The headgroup/chain interface is circular. The average lipid occupies the same volume irrespective of the degree of chain stretching, whether to the side or to the corner of the hexagonal unit cell.

values approaching one. This is a strong indication that the features discussed above, in particular the intensity modulation of the Br distribution, are not artifacts due to for example the limit of resolution. We note that the refinements did not change the phases of the seven independent amplitudes. Therefore Figure 7 is the correct electron density distribution of the Br atoms.

Electron Density Distribution of Lipids in a Unit Cell. As mentioned above, once the phases of Br amplitudes are known, the phase problem of the lipid diffraction is solved (since the sign of the ratio F_0/F_2 has been determined). The same eq 7 can be used to calculate the electron density distribution of the lipid system by replacing F_2 with F_o. The result is shown in Figure 9a,b.

The heaviest atom in a (nonlabeled) phospholipid is the phosphorus. We see a clear phosphate peak at radius 7.3 Å and a bromine peak at radius 18.0 Å (Figure 9b). If we trace the maximum intensity points of the phosphate ring, it is circular within 0.2%. This is consistent with the results of Turner and Gruner[3] who found that at low hydration the water region of the inverted hexagonal phase tends to be circular. Since our lipid system transforms to a distorted hexagonal phase above 50% RH, we could not investigate whether the chain-water interface remains circular or becomes hexagonal at higher hydrations.

Because the amount of water in the sample is unknown, we use the chain region to estimate the number of lipid molecules around the unit cell cylinder. It is known that the distance from the phosphate to the first methylene of the hydrocarbon chains is close to 5 Å.[26] Given the phosphate ring of radius 7.3 Å, the chain region is outside of radius 12.3 Å. We define an average lipid molecule as consisting of 2/3 of di18:0(9−10dibromo)PC
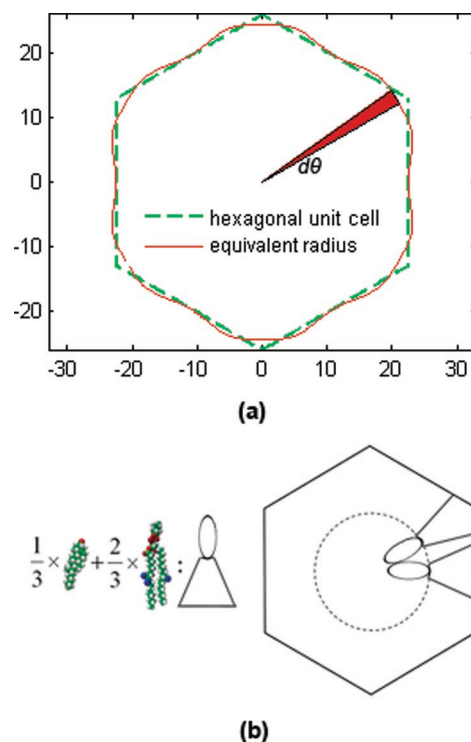
and 1/3 of cholesterol (see Figure 10b). The volumes of various hydrocarbon chains are known.[27] The chain volume of this average lipid is calculated as 875.6 Å³. The radial distance from the interface to the boundary of the unit cell varies from 10.2 Å to 13.7 Å (Figure 9b), with an average of 11.95 Å. Thus, the average cross section of this average lipid is 875.6/11.95 = 73 Å² (the linear dimension of the cross section 8.6 Å). If we take a unit cell cylinder of 8.6 Å in height, its chain region would fit 12.6 average lipids which consist of 8.4 molecules of di18:0(9−10dibromo)PC and 4.2 cholesterol molecules. From the volume within the interface and the volume of the PC headgroup, we find that there are 5.4 water molecules associated with each PC headgroup. This number of water molecules associated with each lipid at 40% RH is consistent with similar estimates by neutron diffraction[4] and NMR[28] measurement on the inverted hexagonal phase of diphytanoyl phosphatidylcholine.

Once the molecular composition of the unit cell is determined, we can put the electron density distributions of Br and of the whole lipid in an absolute scale. The experimental electron densities are related to the real densities by three parameters a, b and b': $\rho^{Br}_{exp} = a\rho^{Br} + b$ and $\rho^{lipid}_{exp} = a\rho^{lipid} + b'$. The three

(26) (a) McIntosh, T. J.; Simon. S. A. *Biochemistry* **1986**, *25*, 4948−4952. (b) Nagle, J. F.; S. Tristram-Nagle, S. *Biochim. Biophys. Acta* **2000**, *1469*, 159−195. (c) Hung, W. C.; Chen, F. Y. *Chin. J. Phys.* **2003**, *41*, 85−91.

(27) Armen, R. S.; Uitto, O. D.; Feller, S. E. *Biophys. J.* **1998**, *75*, 734−744.
(28) Hsieh, C. H.; Sue, S. C.; Lyu, P. C.; Wu, W. G. *Biophys. J.* **1997**, *73*, 870−877.

parameters were determined by the following three conditions: (1) Br electron density vanished in the water region at the center of the unit cell, (2) the integration of ρ_{exp}^{Br} over a unit cell cylinder of 8.6 Å in height equals to the total number of Br electrons in the same volume (or in 12.6 average lipids), (3) the integration of ρ_{exp}^{lipid} over a unit cell cylinder of 8.6 Å in height equals to the total number of electrons in 12.6 average lipids plus 45 water molecules. The electron density maps in Figures 7 and 9 have been normalized by this method.

How Do the Lipids Pack the Hexagonal Unit Cell? We assume that di18:0(9−10dibromo)PC and cholesterol are homogeneously mixed. As we will see below, this assumption is justified by the result of analysis. Using the average lipid defined above that is composed of 2/3 phospholipid and 1/3 cholesterol and therefore carries $2/3 \times 4 = 8/3$ Br atoms, we can use the θ-dependence of the Br distribution to investigate how the lipid chains pack the unit cell.

As noted above (Figure 9b), the radial chain length varies significantly from 10.2Å (toward the side of the hexagon) to 13.7Å (toward the corner). The hexagonal corner is an interstitial region where the chains of three lipid monolayers meet. It is generally believed that there is an energy penalty for the chains to fill or pack the interstitial region as compared with the bilayerlike chain packing along the hexagonal sides.[3,13,29] We shall call this excessive energy the interstitial energy. It is highly desirable to estimate this energy cost. For example, if the interstitial energy is comparable to the bending energy of the interface, one would expect the interface to deviate from being circular so as to lessen the differentials in the chain extension. If the interstitial energy is comparable to the chain compressibility energy, one would expect a density variation around the unit cell. It has long been recognized that during membrane fusion, when two lipid bilayers merge to one, the intermediate lipid structures must include hydrophobic interstices.[3,29] The interstitial energy has been a main source of uncertainties in the study of the energy pathway for membrane fusion.[10,29]

The number of chains distributed between θ and $\theta + d\theta$ is proportional to

$$I(\theta, d\theta) = \int_0^{r_{max}} \rho_{exp}^{Br}(r,\theta) d\theta r dr \qquad (10)$$

Let $I(\theta, d\theta)$ equal to an equivalent area $R*(\theta)^2 d\theta/2$. We found that the equivalent radius $R*(\theta)$ is approximately proportional to the radial distance to the boundary of the unit cell (Figure 10a). This means that each chain occupies the same area in the plane of cylindrical cross section (or the same volume in unit cell) irrespective of the degree of stretching. At the interstitial corner the chains are stretched the longest, therefore have the smallest chain cross section, but its chain volume remains the same as those chains stretched toward the side of the hexagon (Figure 10b). Consequently, the number of chains per angle θ is the highest in the direction toward the corner. This explains the height undulation of the Br distribution we observed in Figure 7.

Thus the lipid chains appear to pack the hexagonal unit cell at constant volume per chain, with no detectable effect from a high-energy interstitial region.

Conclusions

We have for the first time solved the phase problem for diffraction from a nonlamellar lipid structure by the MAD method. The technique of MAD analysis for lipid structures is significantly different from that for protein crystals. We have reconstructed the electron density distribution of the inverted hexagonal phase of a lipid system. We have found that the lipid chains pack the hexagonal unit cell with a simple rule of constant volume per chain, with no detectable effect from a high-energy interstitial region. Each chain occupies the same volume irrespective of the degree of stretching. This is an important finding for the consideration of the energetics of the membrane fusion intermediate states.

(29) Siegel, D. P. *Biophys. J.* **1993**, *65*, 2124−2140.